Expression of miR-200c corresponds with increased reactive oxygen species and hypoxia markers after transient focal ischemia in mice

Arvola, Oiva

2021-10

Arvola , O , Griffiths , B , Rao , A , Xu , L , Pastroudis , I-A & Stary , C M 2021 , ' Expression of miR-200c corresponds with increased reactive oxygen species and hypoxia markers after transient focal ischemia in mice ' , Neurochemistry International , vol. 149 , 105146 . https://doi.org/10.1016/j.neuint.2

http://hdl.handle.net/10138/352047
https://doi.org/10.1016/j.neuint.2021.105146

HHS Public Access

Author manuscript

Neurochem Int. Author manuscript; available in PMC 2022 October 01.

Published in final edited form as:

Neurochem Int. 2021 October ; 149: 105146. doi:10.1016/j.neuint.2021.105146.

Expression of miR-200c corresponds with increased reactive oxygen species and hypoxia markers after transient focal ischemia in mice

Oiva Arvola[1,2,4], **Brian Griffiths**[1], **Anand Rao**[1], **Lijun Xu**[1], **Iason-Alexander Pastroudis**[3], **Creed M. Stary**[1,*]

[1]Department of Anesthesiology, Perioperative & Pain Medicine, Stanford University School of Medicine, Stanford, CA, USA

[2]Division of Anaesthesiology, Jorvi Hospital, Department of Anaesthesiology, Intensive Care and Pain Medicine, University of Helsinki and Helsinki University Hospital, Helsinki, Finland

[3]Department of Anesthetics, Pain Medicine and Intensive Care, Imperial College London, UK

[4]Stem Cells and Metabolism Research Program, Research Programs Unit, Faculty of Medicine, University of Helsinki, Helsinki, Finland

Abstract

Embolic stroke results in a necrotic core of cells destined to die, but also a peri-ischemic, watershed penumbral region of potentially salvageable brain tissue. Approaches to effectively differentiate between the ischemic and peri-ischemic zones is critical for novel therapeutic discovery to improve outcomes in survivors of stroke. MicroRNAs are a class of small non-coding RNAs regulating gene translation that have region- and cell-specific expression and responses to ischemia. We have previously reported that global inhibition of cerebral microRNA-200c after experimental stroke in mice is protective, however delineating the post-stroke sub-regional and cell-type specific patterns of post-stroke miR-200c expression are necessary to minimize off-target effects and advance translational application. Here, we detail a novel protocol to visualize regional miR-200c expression after experimental stroke, complexed with visualization of regional ischemia and markers of oxidative stress in an experimental stroke model in mice. In the present study we demonstrate that the fluorescent hypoxia indicator pimonidazole hydrochloride, the reactive-oxygen-species marker 8-hydroxy-deoxyguanosine, neuronal marker MAP2 and NeuN, and the

[*]**Correspondence:** Creed Stary, MD, PhD, 300 Pasteur Drive, Stanford, CA 94305, cstary@stanford.edu.

CRediT Author Statement

Oiva Arvola: Conceptualization, Methodology, Writing- Reviewing and Editing, Investigation Funding acquisition **Brian Griffiths**: Formal analysis, Writing- Original draft preparation, Funding acquisition. **Anand Rao**: Formal analysis, Writing- Original draft preparation. **Lijun Xu**: Resources, Methodology, Investigation.: **Iason-Alexander Pastroudis**: Investigation, Resources. **Creed Stary**: Conceptualization, Methodology, Funding acquisition, Project administration, Writing- Reviewing and Editing.

Declaration of Interest

All authors certify that they have no affiliations with or involvement in any organization or entity with any financial interest or non-financial interest in the subject matter or materials discussed in this manuscript.

reactive astrocyte marker GFAP can be effectively complexed to determine regional differences in ischemic injury as early as 30 mins post-reperfusion after experimental stroke, and can be effectively used to distinguish ischemic core from surrounding penumbral and unaffected regions for targeted therapy. This multi-dimensional post-stroke immunofluorescent imaging protocol enables a greater degree of sub-regional mechanistic investigation, with the ultimate goal of developing more effective post-stroke pharmaceutical therapy.

Keywords

Stroke; penumbra; microRNA; in situ hybridization; reactive oxygen species; glia

1 Introduction

Embolic stroke comprises 87% of total stroke cases annually in the United States (Benjamin et al., 2019), resulting in substantial mental and physical disability, as well as financial impact for stroke survivors. Histologically, focal ischemia results in a necrotic core of irrevocable neuronal cell death. However, injured neurons in the peri-ischemic, watershed penumbral region exhibit competing outcomes of either delayed cell death or spontaneous recovery (Baron et al., 2014). This region therefore represents an auspicious therapeutic target to ameliorate injury and improve outcomes in stroke survivors. Unfortunately, distinguishing the ischemic core from surrounding penumbral areas immediately after the ischemic insult is widely accepted as a barrier to effective targeted translational advancement for therapies in stroke (Jickling and Sharp, 2011; Zhang et al., 2017).

MicroRNAs have been implicated as important regulators of post-ischemic injury, and identified as a potential therapeutic target to salvage peri-ischemic brain volume (Ouyang et al., 2015, 2013, 2012; Stary et al., 2016; Stary and Giffard, 2015, 2015; Xu et al., 2015). MicroRNAs (miRs) are a class of non-coding RNAs ~22 nucleotides long that regulate gene translation and have been shown to be promising therapeutic targets in other models of disease(Janssen et al., 2013). Endogenous miR expression can be supplemented or altered with exogeneous mimics and inhibitors (Drury et al., 2017; Hanna et al., 2019). Endogenous miR expression levels can be altered within minutes to hours after injury, and our lab has previously observed that miR-200c expression is substantially (~17 fold) elevated in whole brain as early as 1 hr after middle cerebral artery occlusion (MCAO) in mice, only to return to near-baseline levels 24 hr post-injury (Stary et al., 2015). We further demonstrated that pre-injury treatment with intracerebroventricular (ICV) injection with miR-200c antagomir was protective, suggesting that early inhibition of the miR-200c response to stroke may be a potential therapeutic avenue. Novel miR-based therapies have recently been effectively employed for liver disease (Bader, 2012; Janssen et al., 2013). However, miR-expression patterns and biological activity are cell-type dependent (Halushka et al., 2018) and the regional and cell-type specific expression patterns of miR-200c and other potential therapeutic miR targets in the early-immediate response to MCAO remain a critical gap limiting potential off-target effects of anti-miR based therapies for stroke.

To better identify regional distribution of ischemia in experimental stroke, researchers have traditionally relied on tissue staining techniques such as Cresyl violet in fixed tissue, or triphenyltetrazolium chloride (TTC) in metabolically active fresh tissue. However, tissue staining eliminates opportunities for concurrent fluorescent protein staining (Türeyen et al., 2004), and the reliance on tissue degradation or loss of metabolism for these approaches requires a post-injury period of ~24 hr, when miR-200c levels have returned to baseline. Fluoro-Jade staining has been utilized for co-visualization of neurodegeneration with protein, but the highest reported efficacy is 24 hr after injury (Liu et al., 2009). Additionally, multiple markers of apoptotic and necrotic cell death including deoxynucleotidyltransferase-mediated dUTP-biotin nick-end labeling (TUNEL), propidium iodide, caspase 3, Annexin V (Zille et al., 2012), HSP72, and HSP27 (Popp et al., 2009) used to study ischemia-reperfusion injury have not been demonstrated as sufficient for distinguishing the ischemic core from peri-ischemic penumbral regions of the brain in the immediate aftermath of stroke. Alternatively, immunohistochemical (IHC) approaches to visualize infarct volume have utilized degradation of specific brain proteins, for example with microtubule associated protein-2 (MAP2, (Dawson and Hallenbeck, 1996) or sigma-1 receptor protein (Zhang et al., 2017). Notably, the neuronal marker NeuN has been observed to lose immunoreactivity in the ischemic core 1.5 hr after stroke. However, early loss of protein expression may not reliably reflect the early-immediate post-stroke period, and whether loss of NeuN expression is an indication of neuronal cell death or is a result of degradation in antigen-antibody binding remains controversial (Liu et al., 2009; Ünal-Çevik et al., 2004).

Pimonidazole hydrochloride (HypoxyprobeTM) is a commercially available hypoxia indicator capable of penetrating the blood brain barrier (BBB; Li et al., 2018), which limits the diffusion of hydrophilic molecules but allows diffusion of lipophilic or uncharged small molecules from circulation into the central nervous system. Ischemia with and without reperfusion disrupts the BBB, causing edema, hemorrhagic transformation, and exacerbates the brain injury (Liu et al., 2011). The oxidative metabolism of pimonidazole is regulated by NADH and NADPH redox states. Under normoxic conditions the compound is continually in balance between a reduced nitroradical anion intermediate and oxidation by molecular oxygen, however during hypoxia, pimonidazole remains reduced and irreversibly binds to thiols thereby serving as a persistent tissue indicator of hypoxia (Arteel et al., 1998). Pimonidazole hydrochloride has a half-life of ~20 mins in mice and can be reliably assessed several half-lives after intravenous injection using fluorescent IHC. Pimonidazole hydrochloride therefore represents a promising compound to regionally co-localize the degree of brain ischemia with cell-type specific protein or gene expression in the immediate period after cerebral ischemia. Therefore, the aim of the current study was to establish a reproducible methodological approach to assess cell-type-specific miR expression in the acute post-injury period after experimental stroke, with the underlying goal to distinguish the early formation of ischemic core and peri-ischemic penumbra and enable targeted therapies.

2 Materials and Methods

2.1 Equipment and Reagents:

- Hybridization incubator oven (Innova 4200 incubator shaker, Brunswick Corporation, IL, USA)
- Immuno-Stain Moisture Chamber, Black (#240–9020-Z10, Evergreen Scientifics, CA, USA
- Vibratome (Leica VT100S, Leica Biosystems, Germany)
- Zeiss Axio Imager M2 (Carl Zeiss AG) upright fluorescent microscope with ApotomeTM 2.0
- Diethylpyrocarbonate (DEPC, Applichem, Darmstadt, Germany, Catalog # A0881)
- TRIS (Amresco LLC, Solon, OH, USA, Catalog # 0497)
- Phosphate buffered saline (PBS, 10x, Thermo Fisher Scientific, MA, USA, Catalog # 70011044)
- Sodium Chloride (Fisher Scientific, Fair Lawn, NJ, USA, Catalog # S271)
- Hydrochloric Acid (12 M) (Fisher Scientific, Catalog # A144-212)
- Ultrapure 20X saline-sodium citrate (SSC) (Invitrogen, Carlsbad, CA, USA, Catalog # 15557)
- Tyramide signal amplification (TSA) kit (Perkin Elmer, Shelton, 119 CT USA, Catalog #NEL745001KT)
- LNA probes (Exiqon, Woburn, MA, USA), specific for target miRNAs as well as positive and negative controls. We used snRNA U6 as positive control and a scrambled probe with no complementarity to any known miRNAs as negative control (Supplemental Data).
- Primary and secondary antibodies for IHC
- Citric acid (Fisher Scientific, Catalog # BP339-500)
- Sodium Citrate (Fisher Scientific, Catalog # BP327-500)
- 1-methylimidazole (Sigma-Aldrich, Saint Louis, MO, USA, Catalog # 336092)
- (3-Dimethylaminopropyl)-N′-ethylcarbodiimide hydrochloride (EDC, Sigma-Aldrich, Catalog # E1769)
- Glycine (Sigma-Aldrich, Catalog # G7126)
- RNaseZAP (Ambion, Life technologies, NY, USA, Catalog # AM9780)
- Bovine Serum Albumin (BSA), Fraction V—Standard Grade (Gemini Bio-Products, CA, USA, Catalog #700-100P)
- H_20_2 30% (Sigma-Aldrich, Catalog #216763-100ML)

2.2 Solutions:

- Washing buffer I (4× SSC, 0.1% Tween-20)

  To prepare 1 L of buffer, add 200 ml of 20× SSC to 799 ml of water and 1,000 µl of Tween-20. Store at room temperature.

- Washing buffer II (2× SSC)

  To prepare 1 L of buffer, add 100 ml of 20× SSC to 900 ml of autoclaved Millipore (Milli-Q) H2O. Store at room temperature.

- Washing buffer III (1× SSC)

  To prepare 1 L of buffer, add 50 ml of 20× SSC to 950 ml of autoclaved Milli-Q H2O. Store at room temperature.

- Washing buffer IV (0.2× SSC)

  To prepare 1 L of buffer, add 10 ml of 20× SSC to 990 ml of autoclaved Milli-Q H2O. Store at room temperature.

- Sodium citrate buffer (SSC 0.01 M, pH = 6.4): Add 41 mL of 0.1 M sodium citrate to 9 mL of 0.1 M citric acid. Bring the volume up to 500 mL with DEPC-treated H2O or autoclaved dH2O. Store at 4°C.

- TN buffer (0.1 M Tris-HCl pH 7.5, 0.15 M NaCl)

  Add 100 ml of 1-M Tris-HCl and 100 ml of 1.5-M NaCl to 800 ml of autoclaved Milli-Q H2O.

- TNB blocking buffer (0.1-M Tris-HCl pH 7.5, 0.15-M NaCl, 0.5% wt/vol blocking reagent)

  Dissolve 0.5-g blocking reagent in 100-ml TN buffer. Heat gradually to 50–60°C with continuous stirring to completely dissolve the blocking reagent. Prepare aliquots and store the working solution at 4°C. For long-term use, store aliquots at −20°C.

- TNT buffer (0.1-M Tris-HCl pH 7.5, 0.15-M NaCl, 0.2% vol/vol Triton X-100)

  Add 100 ml of 1-M Tris-HCl, 100 ml of 1.5-M NaCl and 20 ml of 10% (vol/vol) Triton X-100 complete with autoclaved Milli-Q H2O up to 1,000 ml.

- Blocking solution for IF (5% NDS in PBS-Triton)

  5ml: add 0.1g of BSA to and 250 uL of normal donkey serum to 4750uL PBS-T.

- −0.2% (w/v) glycine in PBS

  Add 0.02g of glycine in 10mL of PBS.

- −25% Dextran sulfate

  Dissolve 25 g of dextran sulfate sodium salt in H2O to a final volume 165 of 100 ml by stirring.

- Hybridization buffer (10% dextran sulfate in 4× SSC)

To prepare 10 ml, add 2 ml of 20× SSC, 4 ml of dextran sulfate 25% and 4 ml of H2O.

- DEPC-treated water or autoclaved dH2O

  Add 1 mL of DEPC per 1 L of H2O (0.1% v/v). Incubate overnight with gentle agitation and autoclave 170 for 30 min to hydrolyze DEPC. Store at room temperature.

- NaCl (3 M)

  Dissolve 87.8 g of NaCl in 500 mL of DEPC treated H2O.

- Tris-HCl (1 M)

  Dissolve 121.1 g of Tris base in 800 mL of DEPC treated H2O. Adjust pH by adding 12 M HCl. For combined FISH and IF experiments Tris-HCl at both pH 7.4 and 8.0 need to be prepared.

- −10X Tris Buffered Saline

  410 ml of DEPC-treated H2O, 500 ml of 1 M Tris-HCl pH 7.4, 90 g of NaCl.

- Sodium citrate (0.1 M)

  14.705 g of sodium citrate in 500 mL of DEPC-treated autoclaved dH2O. Store at 4°C.

- Citric acid (0.1 M)

  9.56 g of citric acid in 500 mL of DEPC-treated autoclaved dH2O. Store at 4°C.

- Prehybridization buffer (3% BSA in 4× SSC)

  to prepare 10 ml, add 0.3 g of Bovine Serum Albumin to 10 ml of 4× SSC.

- H202 3% in PBS

  Add 1ml of H202 30% to 9ml of PBS.

2.3 Methods

2.3.1 Animal Care—This study was carried out in accordance with the recommendations of with NIH guidelines for humane animal treatment (NIH Publications No. 80–23, revised 1978). All efforts were made to minimize animal suffering, and to reduce the number of animals used. The protocol was approved by the Stanford University Animal Care and Use Committee. All mice were housed in a research animal facility room at 22 ± 2°C on a 12-hr light-dark cycle with ad libitum access to food and water.

2.3.2 Experimental Protocol—Young domestic male C57BL/6 mice (age 8–10 weeks, Jackson Laboratory, Sacramento, CA) were randomly assigned to receive intracerebroventricular (ICV) pre-treatment of either miR-200c antagomir or mismatch-control sequence infusion 24 hrs before undergoing 1 hr middle cerebral artery occlusion (MCAO). The animals received intravenous injection of pimonidazole hydrochloride (PimonidazoleTM, HP1-100Kit, Pimonidazole Inc, MA, USA) 5 (n=24) or 90 mins (n=6)

prior to MCAO and were sacrificed at 30 mins or 2 hrs of reperfusion for analysis of ischemic brain regions.

2.3.3 Stereotactic Injections—All mice (n = 31) were anesthetized with ventilated 2%–2.5% isoflurane and placed in stereotaxic frame for intracerebroventricular (ICV) injection of miR-200c antagomir or mismatch-control sequence as we have performed previously (Stary et al., 2015). Briefly, the animals were placed in a stereotaxic frame and a 26g brain infusion cannula was introduced into the left lateral ventricle following coordinates: bregma: − 0.58 mm; dorsoventral: 2.1 mm; lateral: 1.2 mm, as previously described [2]. After 20-minute infusion of 3 pmol/g body weight in 2 μL of miR-200c antagomir (miRCURY LNA™ miRNA Custom Power Inhibitor 200C_1, Cat. No. YCI0202184-DDB, Qiagen, Germany) or mismatch-control (miRCURY LNA miRNA Power inhibitor negative control A, Cat. No. YCI0199006-111, Qiagen, Germany) mixed with cationic lipid DOTAP (4μl; 6 μl total volume; Roche) the head wound was closed, and mice weaned from anesthesia.

2.3.4 Experimental Stroke and Intravenous Pimonidazole Hydrochloride Injection—Mice (n=25) were subjected to 1h MCAO as previously described (Ouyang et al., 2012; Stary et al., 2015). Briefly, animals were randomized to treatment group by coin flip and then anesthetized with 2% isoflurane and secured; temperature and respiratory rate were monitored continuously, and rectal temperature was maintained at 37 ± 0.5 °C with homeothermic blanket (Harvard Apparatus, MA, USA). A subcutaneous buprenorphine injection (1.0 mg/kg) prior to incision was used as analgesic. Jugular veins were exposed for pimonidazole hydrochloride in saline injection (60mg/kg at 30mg/mL) or saline injection alone, either 90 mins or 5 mins prior to 1h MCAO *via* silicone-coated 6–0 monofilament thread. Sham-operated mice (n=5) underwent ligation of the external carotid artery but no suture insertion.

2.3.5 Tissue Collection and Processing—Brains were collected at 30 mins (miR-200c antagomir group n=6, mismatch control group n=7, sham infarction n=2) or 2 hrs (miR-200c antagomir group n=7, mismatch control group n= 6, sham infarction group n=3) after reperfusion for immunohistochemical assessment. While deeply anesthetized, mice underwent transcardiac perfusion with ice cold saline, followed by ice cold 4% paraformaldehyde (PFA). The brains were then submerged in 4% PFA for 48 hrs. Brains were then cut with a vibratome in 50 μM thick sections (Leica VT100S, Leica Biosystems, Germany) and stored in phosphate buffered saline (PBS). One mouse died after the ICV infusion (mismatch at 30 mins), and was excluded from the study, leading to 30 min mismatch control group of 6.

2.3.6 Fluorescence Immunohistochemistry—Sections from the hippocampal plane (−1.2 to −2.0 mm Anterior Commissure) were selected for imaging to allow assessment of both cortical and subcortical regions. Free-floating sections were first washed in PBS twice for 15 mins at room temperature prior to blocking endogenous peroxidases by submerging in 3% H_2O_2 in PBS for 45 mins. After a 15 min permeabilization step in 0.2 % Triton x-100 in PBS, the sections were washed for 15 mins in PBS, then blocked with 5% donkey

serum (#D9663-10ML, Sigma-Aldrich, MO, USA) in PBS at 4°C overnight. The sections were then washed with PBS three times for 15 mins at room temperature the following day, followed by serial fluorescent staining beginning with incubation in primary antibody solutions consisting of: 1) Pimonidazole Mouse-AB, [1:100], #HP1-100Kit, Pimonidazole™ Inc; 2) Goat-8-OHdG, [1:200], #ab10802, Abcam, Cambridge, United Kingdom; 3) Chicken-MAP2 [1:200] #ab5392, Abcam; 4) Rabbit-NeuN [1:500] #NBP1-77686, Novus Biologicals, CO, USA; and, 5) Chicken-GFAP[1:500] #ab4674, Abcam in 3% filtered (0.2 micron filter) bovine serum albumin (BSA) in PBS at 4°C, overnight. The following day the sections were washed three times in PBS for 15 mins, followed by secondary antibody solutions: 1) Donkey anti-Goat, Alexa Fluor 594, [1:200], # A-11058 Invitrogen, NY, USA; 2) Donkey anti-Mouse, Alexa Fluor 488, [1:200], #A-21202,Invitrogen; 3) Donkey anti-Chicken, Alexa Fluor 647 [1:500], #703-606-155, Jackson Immunoresearch Laboratories Inc, PA, USA; 4) Donkey-anti-Rabbit, Alexa Fluor 594 [1:500] #A21207, Abcam), and, 5) 4′,6-diamidino-2-phenylindole-hydrochloride (DAPI) [1:1000] #1700624 Life Technologies, CA, USA, in PBS at 4°C, overnight. On the final day, the sections were washed with PBS three times for 15 mins prior to mounting with ProLong™ Glass Antifade Mountant (#P36980, Fisher Scientific, NH, USA) to Fisherbrand™ Superfrost™ Plus Microscope Slides (#22-037-246, Fisher Scientific). An observer blinded to treatment group quantified 4 sections/brain using 50 μm coronal sections stained with pimonidazole hydrochloride, MAP2, DAPI, 8-OHdG

2.3.7 Complexing miR-200c FISH and fluorescent IHC—In order to determine the cell-type specific expression of miR-200c at baseline, 30 mins and 2h post MCAO we combined fluorescent *in situ* hybridization (FISH) with fluorescent IHC for neuronal markers (NeuN, MAP2) and the astrocyte marker (GFAP), an oxidative stress markers (8-OHdG) and DAPI. Briefly, a double FAM-labeled miR-200c-5p miRCURY LNA miRNA detection probe (#YD00611801-BED, Qiagen, NJ, USA) was used in combined protocols described by Chaudhuri *et al.* (Datta Chaudhuri et al., 2013) and de Planell-Saguer *et al* (de Planell-Saguer et al., 2010)[3] with minor modifications and optimization steps described here: 1) sections were hybridized overnight at 44 °C; 2) stringency washes were performed at 51 °C for 15 min each; 3) additional stringency wash of 0.2x SSC at 51 °C for 30min; and, 4) all PBS washes were performed for 5 min each. All sections were imaged using a Zeiss Axio Imager M2 (Carl Zeiss AG) with Apotome 2.0 with Neurolucida (MBF Bioscience) software, version 2017.03.2. Small nuclear RNA U6 was used as positive control and a scrambled probe with no complementarity to any known miRNAs was used as negative control (Supplemental Data 1).

2.3.8 Image Processing—All images were processed using ImageJ (1.51s, Java 1.8.0_66, (64-bit), National Institutes of Health, MD, USA). Four images of each brain section were imaged with a fixed illumination intensity using a 2.5x Nikon Neofluar objective for whole section imaging. The four images of each brain were combined *in silico* using pairwise stitching feature by ImageJ (Fusion method set to Linear blending, Check peaks = 5, compute overlap, registration channel selected to DAPI for all sections). Cell-type specific miR-200c expression was assessed with a fixed illumination intensity using a 40x air Nikon ApoChromat objective in regions of core or penumbra.

2.3.9 Statistical Analysis—All brain sections were stained three times as technical replicates to ensure proper, reproducible staining results. IBM SPSS Statistics 24 (version 24 64-bit edition, IBM, NY, USA) was used for statistical analyses. All data reported are mean ± standard error of the mean. Statistical analysis was performed using independent samples t-tests for two groups, and ANOVA with Bonferroni post-test for comparisons of more than two groups and testing for interactions. A p-value of < 0.05 was considered significant.

3 Results

The mean weight of mice was 26.3 g (SD = 2.29) with no differences between the study groups. No differences were observed in body temperature, surgical procedure times, nor time under anesthesia between the study groups (data not shown).

3.1 Ischemic core and penumbra can be clearly delineated at 30 mins after MCAO

Fluorescent labeling with pimonidazole hydrochloride was strong in all ischemic samples (Figs. 1A, 1B). Co-labeling pimonidazole with MAP2 IHC was used to assess MAP2 loss within ischemic regions (Figs. 1A, 1B). Changes in MAP2 expression has previously been utilized to determine ischemic core from perilesional zones as early as 2 hrs post-reperfusion (Popp, et al. 2009). Pimonidazole fluorescence at 30 mins post-reperfusion only partially overlapped loss of MAP2 expression after ischemia (Fig. 1B). Pimonidazole staining consistently followed the known anatomical vasculature (Xiong et al., 2017) and stained most of the cortex, lateral thalamic and hypothalamic regions, hippocampus, and striatum (Figs. 1C). Significantly greater levels of pimonidazole fluorescence were demonstrated in the ipsilateral hemisphere in the cortex ($p<.001$), hippocampus ($p<.001$), hypothalamus ($p=.004$), amygdala ($p=.008$) and the striatum ($p=.021$) relative to the same regions in the contralateral hemisphere (Figs. 1C, 1D). There was no apparent effect of microRNA-200c inhibitor treatment or recovery time on pimonidazole labeling (Figs. 2A, 2B). Furthermore, injecting pimonidazole 5 min or 90 min prior to MCAO did not affect the ability to determine the hypoxic areas, although comparatively, the staining illumination was greater when injected 5 min prior to surgery (Supplemental Data 2). During hypoxia, pimonidazole remains reduced and irreversibly binds to thiols thereby serving as a persistent tissue indicator of hypoxia. The central advantage of pimonidazole is that after ischemic injury fluorescence does not change with the physiologically evolving core and penumbral regions.

3.2 Co-visualizing ischemic regions and areas of oxidative stress with miR-200c expression

Sections were stained with both pimonidazole and 8-hydroxy-2’-deoxyguanosine (8-OHdG) to visualize ischemic regions and formation of reactive oxygen species (ROS, Figs. 2C, 3). Notably, at 2 hrs after MCAO, areas with clear borders of high pimonidazole fluorescence (core) coincided with low 8-OHdG fluorescence, while in adjacent regions high 8-OHdG fluorescence was observed with low pimonidazole fluorescence (penumbra, Fig. 3A). However, this observed effect was not consistent across all regions, and less so at 30 minutes after MCAO (Fig 2C). These observations suggest that the highest ROS production may actually occur in peri-ischemic and mildly ischemic regions relative to severely ischemic regions, which may be a function of profound mitochondrial dysfunction and loss of cell

viability in the core. Co-localization of miR-200c, however, indicated greater qualitative levels of expression in penumbra relative to core (Fig. 3B).

We extended these observations to assess whether miR-200c antagomir altered regional levels of ROS production after MCAO. Based on our prior observations that high ROS production does not regionally co-localize with ischemic core (Figs. 2C, 3A) and therefore may not correlate with severity of injury, we stratified severity of ischemia based on pimonidazole fluorescence intensity (Fig. 4A) as ‘severe’ or ‘mild’ injury by using a 16-color LUT in ImageJ (Fig. 4A). This was done by assessment of signal intensity, which was significantly lower in ‘mild’ regions when compared to ‘severe’ regions (Fig. 4B) but consistently higher than sham signal. Uninjured hemispheres did not demonstrate any significant variation in signal intensity. Next, we analyzed mild and severe regions for MAP2 and 8-OHdG staining, and quantified regional signal intensities. Animals treated with microRNA-200c inhibitor demonstrated a significant reduction in 8-OHdG signal in areas of mild injury when compared to control after 2 hrs post-MCAO reperfusion (Fig. 4C). Neither the mildly nor severely injured regions demonstrated significant differences in the MAP2 staining (data not shown).

3.3 Cell-type specific and regional post-MCAO miR-200c expression

We analyzed cell-type specific miR-200c expression in select ischemic and corresponding non ischemic contralateral regions by complexing pimonidazole and cell-type specific IHC markers with miR-200c FISH. MAP2 immunogenicity was visible in some cortical regions with high pimonidazole intensity (Fig. 5A), yet hippocampal, ventral and posterolateral thalamic regions demonstrate no MAP2 loss, despite pimonidazole fluorescence. Conversely, the expression of miR-200c in the ischemic core was generally decreased compared to penumbral regions (Figs. 5A,B). Notably, loss of NeuN immunogenicity and miR-200c fluorescence in ischemic regions appeared co-localize in cortex, thalamus and hippocampus (Fig. 5B).

In order to further assess cell-type specific expression of miR-200 in response to MCAO we assessed cell-type specific expression in the peri-ischemic hippocampus and the non-ischemic contralateral side for control comparison (Fig. 6). The non-ischemic hippocampal subregions CA1-CA3 and DG expressed notable miR-200c, but CA1-CA3 regions consistently demonstrated diminished miR-200c expression and loss of NeuN antigenicity (Figs 6A, Supplemental data 3) which is in agreement with established understanding of hippocampal sub-regional differences in response to ischemia (Stary et al., 2016). In contralateral hippocampus, miR-200c expression was greatest in NeuN+ neurons relative to GFAP+ astrocytes (Fig. 6B). However, in the ipsilateral hippocampus, astrocyte miR-200c expression was notably increased relative to the contralateral side, while neuronal miR-200c appeared to decrease in parallel with loss of NeuN signal intensity (Fig. 6C). Semi-quantitative analysis (Fig. 6D) of miR-200c fluorescence in astrocytes (GFAP+) and neurons (NeuN+) suggested a trend ($p = 0.52$, $n=4$) towards augmented miR-200c in astrocytes 2 hrs after MCAO but not in neurons. This may be related to an associated loss of NeuN (Fig. 6D).

1. Discussion

Improvement in stroke research relies on the ability to distinguish the necrotic infarct core from potentially salvageable peri-ischemic penumbra. We present here a novel approach to visualize the distinct ischemic regions in the brain as early as 30 mins in a stroke model. Pimonidazole fluorescence was detectable throughout the predicted area of infarct, and absent from the contralateral, uninjured hemisphere, demonstrating its utility as a regional marker for acute ischemia-reperfusion injury. We interpret the differential intensity of pimonidazole to delineate early core and penumbral regions. Our findings also suggest that MAP2 is not a sufficient marker for early-stage infarct: MAP2 immunoreactivity loss was only observed in severe ischemic regions with cellular degradation immediately after MCAO.

Another feature of pimonidazole was its ability to highlight distinct ischemic regions with discrete ischemic/peri-ischemic boundaries. However, even within areas generally represented as mild ischemia we observed regions of pimonidazole signal heterogeneity, likely corresponding to sub-regional differences in blood flow distribution. Utilizing a semi-quantitative approach to counter biased analysis and subjectivity we also observed that the severity of ischemic injury did not directly correlate with ROS production using the DNA oxidation marker 8-OHdG, which has previously been used as a marker for oxidative damage in stroke (Nakajima et al., 2012). 8-OHdG accumulates in injured cells and its presence implies DNA damage. It is possible that the decreased 8-OHdG fluorescence in the core could be due to diminished mitochondrial function relative to the peri-ischemic regions. 8-OHdG levels have been observed to return to endogenous levels by 45 mins after injury (Hamilton et al., 2001) which may represent a narrow window for this particular marker. Our observation of inconsistencies in 8-OHdG, MAP2 and pimonidazole staining patterns might therefore be due to irreversible pimonidazole binding during ischemia and/or differential susceptibility to ischemic injury between brain regions.

In parallel with 8-OHdG levels, we observed a subsequent relative increase in miR-200c expression in the penumbra, up to 2 hrs post-injury. In contrast, miR-200c expression was absent from the ischemic core. This is in agreement with our previous observations in neuronal cells that oxidative stress results in increased miR-200c levels (Stary et al., 2015). Additionally, in the present study we observed loss of NeuN immunogenicity in hippocampal neurons at 30 mins after MCAO. This might be due to a loss of antigenicity rather than loss of neurons or neuronal degradation (Ünal-Çevik et al., 2004), but is also in agreement with our prior observations that exogenously increasing miR-200c levels results in neuronal cell death (Stary et al., 2015). MiR-200c inhibition *via* antagomir resulted in a reduction in 8-OHdG fluorescence intensity, which corroborates prior observations that *in vivo* miR-200c antagomir treatment decreased MCAO injury severity and improved functional recovery. These observations suggest that peri-ischemic regions with higher miR-200c areas may contain neurons susceptible to delayed cell death (Kozak et al., 2020). Conversely, miR-200c expression was also high in areas that do not experience expansive cell death after MCAO, such as the dentate gyrus and the contralateral hemisphere. Whether this is due to separate protective mechanisms is not clear, however it can be concluded that miR-200c expression alone is insufficient to predict cell death in the penumbra.

MicroRNAs have cell-type specific roles (Guduric-Fuchs et al., 2012), and miR-200c is enriched in the brain, particularly in neurons, oligodendrocytes (Buller et al., 2012; Lau et al., 2008) and microglia (Tang et al., 2017; Yu et al., 2015). MiR-200c expression increases in response to oxidative stress (Lee et al., 2010; Stary et al., 2015) and suppresses MAP2 expression (Yuan et al., 2017). In the present study utilizing this novel complexing method we confirmed a high degree of co-localization with miR 200c and neurons and low miR-200c in astrocytes. However, using a semi-quantitative approach measuring fluorescence intensity we also observed a trend ($p=0.052$) towards increased miR-200c expression in astrocytes but not neurons in response to MCAO. Astrocytes are important mediators of cell death after stroke (Stary and Giffard, 2015). They coordinate neuronal maintenance, neurite outgrowth and repair of the neuronal network (Araque et al., 1999; Benarroch, 2005; Liu and Chopp, 2016), protecting neurons during pathophysiologic stresses such as those from stroke (Takano Takahiro et al., 2009), traumatic brain injury (Shields et al., 2011), or spinal cord injury (Falnikar et al., 2015). Studies targeting astrocytes for improving outcome following cerebral ischemia are promising: augmenting astrocyte glutamate sequestration by increasing the activity of astrocytic glutamate transporter GLT-1 decreased glutamate excitotoxicity (Ouyang et al., 2007; Weller et al., 2008). Overexpression of superoxide dismutase 2 in astrocytes reduced evidence of oxidative stress in the CA1 from transient global ischemia (Xu et al., 2010), and was accompanied by preservation of GLT-1. Furthermore, astrocytes are a potential source of new neurons in injured brains (Griffiths et al., 2019, 2020). Astrocytic mitochondrial function plays several direct and indirect roles in maintaining neuronal survival from ischemic injury (Stary and Giffard, 2015). Mitochondria are central regulators of apoptosis, reactive oxygen species and intracellular Ca^{2+} handling, and increasing astrocytic pyruvate preserves mitochondrial function and improves neuronal survival (Miao et al., 2011). Astrocytes have also been shown to sequestrate degraded neuronal mitochondria (Davis et al., 2014). Notably, astrocytes are capable of direct transfer of functional mitochondria to neurons, and that suppression of this process exacerbates ischemic injury (Hayakawa et al., 2016). Additionally, glial cells transfer microRNAs to neurons through secreted extracellular vesicles modulating inflammatory response to stimuli (Prada et al., 2018). Therefore, the results of this study suggest that inhibiting the increase in miR-200c expression in astrocytes may be a potential therapeutic avenue for salvaging penumbra after stroke, and effectively improving clinical outcome. These observations should be further validated through quantitative means such as fluorescence automated cell counting (FACS) or single-cell RNA sequencing. We also cannot differentiate whether miR-200c expression was definitively cell-type dependent, or related to exosome-mediated inter-cellular miR-200c transfer (Morel et al., 2013; Rooj et al., 2016). Future studies can overcome this limitation by assessing targeted cell-type specific inhibition of miR-200c expression and/or incorporating recently developed high resolution miR labeling techniques (Goryacheva et al., 2018) to track inter-cellular transfer of endogenously expressed miRs in real time and by blocking exosome transfer.

An additional limitation of the present study is that we did not correlate pimonidazole fluorescence with a traditional stain for infarction such as Cresyl violet or TTC. These stains rely on degradation of tissue or total loss of metabolic activity, and are a more

reliable measure for assessment of infarct volume at time points beyond the immediate post-stroke period (Fishbein et al., 1981; Türeyen et al., 2004). Future studies could incorporate protocols incorporating a graded degree of ischemic injury to verify pimonidazole fluorescence correlates with injury severity. A final limitation in the present study is that our traditional fluorescent microscopy approach was limited to only four fluorescent channels per sample, necessitating parallel tissue processing which may have been subject to variability in fluorescence signal intensity. Next-generation High Dimensional Imaging modalities (Goltsev et al., 2018; Schulz et al., 2018) represent a future potential leap to fully exploit multiplexing approaches to more accurately assess post-injury cell-type specific gene expression, a critical hurdle to advance the clinical application of miR-based therapeutic strategies for stroke.

Supplementary Material

Refer to Web version on PubMed Central for supplementary material.

Funding

Finnish Cultural Foundation Grant 00171200 and Finnish Medical Association grant #2776/2019 and Orion Research Foundation sr 12/2020 to OA, American Heart Association (AHA) grant #18POST33990395 to BG, and AHA grant FTF19970029 and NIH grant NS107445 to CS.

Data Availability Statement

Available upon request.

4 References

Araque A, Sanzgiri RP, Parpura V, Haydon PG, 1999. Astrocyte-induced modulation of synaptic transmission. Can. J. Physiol. Pharmacol77, 699–706. 10.1139/y99-076 [PubMed: 10566947]

Arteel GE, Thurman RG, Raleigh JA, 1998. Reductive metabolism of the hypoxia marker pimonidazole is regulated by oxygen tension independent of the pyridine nucleotide redox state. Eur. J. Biochem253, 743–750. 10.1046/j.1432-1327.1998.2530743.x [PubMed: 9654074]

Bader AG, 2012. miR-34 - a microRNA replacement therapy is headed to the clinic. Front. Genet3, 120. 10.3389/fgene.2012.00120 [PubMed: 22783274]

Baron J-C, Yamauchi H, Fujioka M, Endres M, 2014. Selective Neuronal Loss in Ischemic Stroke and Cerebrovascular Disease. J. Cereb. Blood Flow Metab34, 2–18. 10.1038/jcbfm.2013.188 [PubMed: 24192635]

Benarroch EE, 2005. Neuron-Astrocyte Interactions: Partnership for Normal Function and Disease in the Central Nervous System. Mayo Clin. Proc80, 1326–1338. 10.4065/80.10.1326 [PubMed: 16212146]

Benjamin EJ, Muntner P, Alonso A, Bittencourt MS, Callaway CW, Carson AP, Chamberlain AM, Chang AR, Cheng S, Das SR, Delling FN, Djousse L, Elkind MSV, Ferguson JF, Fornage M, Jordan LC, Khan SS, Kissela BM, Knutson KL, Kwan TW, Lackland DT, Lewis TT, Lichtman JH, Longenecker CT, Loop MS, Lutsey PL, Martin SS, Matsushita K, Moran AE, Mussolino ME, O'flaherty M, Pandey A, Perak AM, Rosamond WD, Roth GA, Sampson UKA, Satou GM, Schroeder EB, Shah SH, Spartano NL, Stokes A, Tirschwell DL, Tsao CW, Turakhia MP, Vanwagner LB, Wilkins JT, Wong SS, Virani SS, 2019. Heart Disease and Stroke Statistics-2019 Update A Report From the American Heart Association. 10.1161/CIR.0000000000000659

Buller B, Chopp M, Ueno Y, Zhang L, Zhang RL, Morris D, Zhang Y, Zhang ZG, 2012. Regulation of serum response factor by miRNA-200 and miRNA-9 modulates oligodendrocyte progenitor cell differentiation. Glia60, 1906–1914. 10.1002/glia.22406 [PubMed: 22907787]

Datta Chaudhuri A, Yelamanchili SV, Fox HS, 2013. Combined fluorescent in situ hybridization for detection of microRNAs and immunofluorescent labeling for cell-type markers. Front. Cell. Neurosci7. 10.3389/fncel.2013.00160

Davis CO, Kim K-Y, Bushong EA, Mills EA, Boassa D, Shih T, Kinebuchi M, Phan S,Zhou Y, Bihlmeyer NA, Nguyen JV, Jin Y, Ellisman MH, Marsh-Armstrong N, 2014. Transcellular degradation of axonal mitochondria. Proc. Natl. Acad. Sci111, 9633–9638. 10.1073/pnas.1404651111 [PubMed: 24979790]

Dawson DA, Hallenbeck JM, 1996. Acute Focal Ischemia-Induced Alterations in MAP2 Immunostaining: Description of Temporal Changes and Utilization as a Marker for Volumetric Assessment of Acute Brain Injury. J. Cereb. Blood Flow Metab16, 170–174. 10.1097/00004647-199601000-00020 [PubMed: 8530550]

de Planell-Saguer M, Rodicio MC, Mourelatos Z, 2010. Rapid in situ codetection of noncoding RNAs and proteins in cells and formalin-fixed paraffin-embedded tissue sections without protease treatment. Nat. Protoc5, 1061–1073. 10.1038/nprot.2010.62 [PubMed: 20539282]

Drury RE, O'Connor D, Pollard AJ, 2017. The Clinical Application of MicroRNAs in Infectious Disease. Front. Immunol8. 10.3389/fimmu.2017.01182

Falnikar A, Li K, Lepore AC, 2015. Therapeutically targeting astrocytes with stem and progenitor cell transplantation following traumatic spinal cord injury. Brain Res., Repair stratagies for spinal cord injury1619, 91–103. 10.1016/j.brainres.2014.09.037 [PubMed: 25251595]

Fishbein MC, Meerbaum S, Rit J, Lando U, Kanmatsuse K, Mercier JC, Corday E, Ganz W, 1981. Early phase acute myocardial infarct size quantification: Validation of the triphenyl tetrazolium chloride tissue enzyme staining technique. Am. Heart J101, 593–600. 10.1016/0002-8703(81)90226-X [PubMed: 6164281]

Goltsev Y, Samusik N, Kennedy-Darling J, Bhate S, Hale M, Vazquez G, Black S, Nolan GP, 2018. Deep Profiling of Mouse Splenic Architecture with CODEX Multiplexed Imaging. Cell174, 968–981.e15. 10.1016/j.cell.2018.07.010 [PubMed: 30078711]

Griffiths BB, Bhutani A, Stary CM, 2020. Adult neurogenesis from reprogrammed astrocytes. Neural Regen. Res15, 973–979. 10.4103/1673-5374.270292 [PubMed: 31823866]

Griffiths BB, Ouyang Y-B, Xu L, Sun X, Giffard RG, Stary CM, 2019. Post-injury inhibition of miR-181a promotes restoration of hippocampal CA1 neurons after transient forebrain ischemia in rats. eNeuro.

Guduric-Fuchs J, O'Connor A, Camp B, O'Neill CL, Medina RJ, Simpson DA, 2012. Selective extracellular vesicle-mediated export of an overlapping set of microRNAs from multiple cell types. BMC Genomics13, 357. 10.1186/1471-2164-13-357 [PubMed: 22849433]

Halushka MK, Fromm B, Peterson KJ, McCall MN, 2018. Big Strides in Cellular MicroRNA Expression. Trends Genet. 34, 165–167. 10.1016/j.tig.2017.12.015 [PubMed: 29361313]

Hamilton ML, Guo Z, Fuller CD, Van Remmen H, Ward WF, Austad SN, Troyer DA, Thompson I, Richardson A, 2001. A reliable assessment of 8-oxo-2-deoxyguanosine levels in nuclear and mitochondrial DNA using the sodium iodide method to isolate DNA. Nucleic Acids Res. 29, 2117–2126. 10.1093/nar/29.10.2117 [PubMed: 11353081]

Hanna J, Hossain GS, Kocerha J, 2019. The Potential for microRNA Therapeutics and Clinical Research. Front. Genet10. 10.3389/fgene.2019.00478

Hayakawa K, Esposito E, Wang X, Terasaki Y, Liu Y, Xing C, Ji X, Lo EH, 2016. Transfer of mitochondria from astrocytes to neurons after stroke. Nature535, 551–555. 10.1038/nature18928 [PubMed: 27466127]

Janssen HL, Reesink HW, Lawitz EJ, Zeuzem S, Rodriguez-Torres M, Patel K, van der Meer AJ, Patick AK, Chen A, Zhou Y, Persson R, King BD, Kauppinen S, Levin AA, Hodges MR, 2013. Treatment of HCV infection by targeting microRNA. N. Engl. J. Med368, 1685–1694. 10.1056/NEJMoa1209026 [PubMed: 23534542]

Jickling GC, Sharp FR, 2011. Blood Biomarkers of Ischemic Stroke. Neurotherapeutics8, 349. 10.1007/s13311-011-0050-4 [PubMed: 21671123]

Kozak J, Jonak K, Maciejewski R, 2020. The function of miR-200 family in oxidative stress response evoked in cancer chemotherapy and radiotherapy. Biomed. Pharmacother125, 110037. 10.1016/j.biopha.2020.110037 [PubMed: 32187964]

Lau P, Verrier JD, Nielsen JA, Johnson KR, Notterpek L, Hudson LD, 2008. Identification of Dynamically Regulated MicroRNA and mRNA Networks in Developing Oligodendrocytes. J. Neurosci28, 11720–11730. 10.1523/JNEUROSCI.1932-08.2008 [PubMed: 18987208]

Lee ST, Chu K, Jung KH, Yoon HJ, Jeon D, Kang KM, Park KH, Bae EK, Kim M, Lee SK, Roh JK, 2010. MicroRNAs induced during ischemic preconditioning. Stroke41, 1646–1651. 10.1161/STROKEAHA.110.579649 [PubMed: 20576953]

Li W, Liu H, Qian W, Cheng L, Yan B, Han L, Xu Q, Ma Q, Ma J, 2018. Hyperglycemia aggravates microenvironment hypoxia and promotes the metastatic ability of pancreatic cancer. Comput. Struct. Biotechnol. J16, 479–487. 10.1016/j.csbj.2018.10.006 [PubMed: 30455857]

Liu F, Schafer DP, McCullough LD, 2009. TTC, Fluoro-Jade B and NeuN staining confirm evolving phases of infarction induced by middle cerebral artery occlusion. J. Neurosci. Methods179, 1–8. 10.1016/j.jneumeth.2008.12.028 [PubMed: 19167427]

Liu S, Levine SR, Winn HR, 2011. Targeting ischemic penumbra Part II: selective drug delivery using liposome technologies. J. Exp. Stroke Transl. Med4, 16–23. [PubMed: 21909454]

Liu Z, Chopp M, 2016. Astrocytes, therapeutic targets for neuroprotection and neurorestoration in ischemic stroke. Prog. Neurobiol, Targeting Astrocytes in Brain Injuries: A Translational Research Approach144, 103–120. 10.1016/j.pneurobio.2015.09.008 [PubMed: 26455456]

Miao Y, Qiu Y, Lin Y, Miao Z, Zhang J, Lu X, 2011. Protection by pyruvate against glutamate neurotoxicity is mediated by astrocytes through a glutathione-dependent mechanism. Mol. Biol. Rep38, 3235–3242. 10.1007/s11033-010-9998-0 [PubMed: 20182801]

Morel L, Regan M, Higashimori H, Ng SK, Esau C, Vidensky S, Rothstein J, Yang Y, 2013. Neuronal Exosomal miRNA-dependent Translational Regulation of Astroglial Glutamate Transporter GLT1. J. Biol. Chem288, 7105–7116. 10.1074/jbc.M112.410944 [PubMed: 23364798]

Nakajima H, Unoda K, Ito T, Kitaoka H, Kimura F, Hanafusa T, 2012. The Relation of Urinary 8-OHdG, A Marker of Oxidative Stress to DNA, and Clinical Outcomes for Ischemic Stroke. Open Neurol. J6, 51–57. 10.2174/1874205X01206010051 [PubMed: 22754596]

Ouyang Y-B, Lu Y, Yue S, Xu L-J, Xiong X-X, White RE, Sun X, Giffard RG, 2012. miR-181 regulates GRP78 and influences outcome from cerebral ischemia in vitro and in vivo. Neurobiol. Dis, Assessment of Gene Expression in Neuropsychiatric Disease45, 555–563. 10.1016/j.nbd.2011.09.012 [PubMed: 21983159]

Ouyang Y-B, Stary, C. M, Yang G-Y, Giffard R, 2013. microRNAs: Innovative Targets for Cerebral Ischemia and Stroke. Curr. Drug Targets14, 90–101. 10.2174/138945013804806424 [PubMed: 23170800]

Ouyang YB, Stary CM, White RE, Giffard RG, 2015. The use of microRNAs to modulate redox and immune response to stroke. Antioxid. Redox Signal22, 187–202. 10.1089/ars.2013.5757 [PubMed: 24359188]

Ouyang Y-B, Voloboueva LA, Xu L-J, Giffard RG, 2007. Selective Dysfunction of Hippocampal CA1 Astrocytes Contributes to Delayed Neuronal Damage after Transient Forebrain Ischemia. J. Neurosci27, 4253–4260. 10.1523/JNEUROSCI.0211-07.2007 [PubMed: 17442809]

Popp A, Jaenisch N, Witte OW, Frahm C, 2009. Identification of Ischemic Regions in a Rat Model of Stroke. PLOS ONE4, e4764. 10.1371/journal.pone.0004764 [PubMed: 19274095]

Prada I, Gabrielli M, Turola E, Iorio A, D'Arrigo G, Parolisi R, De Luca M, Pacifici M, Bastoni M, Lombardi M, Legname G, Cojoc D, Buffo A, Furlan R, Peruzzi F, Verderio C, 2018. Glia-to-neuron transfer of miRNAs via extracellular vesicles: a new mechanism underlying inflammation-induced synaptic alterations. Acta Neuropathol. (Berl.)135, 529–550. 10.1007/s00401-017-1803-x [PubMed: 29302779]

Rooj AK, Mineo M, Godlewski J, 2016. MicroRNA and extracellular vesicles in glioblastoma – Small but powerful. Brain Tumor Pathol. 33, 77–88. 10.1007/s10014-016-0259-3 [PubMed: 26968172]

Schulz D, Zanotelli VRT, Fischer JR, Schapiro D, Engler S, Lun X-K, Jackson HW, Bodenmiller B, 2018. Simultaneous Multiplexed Imaging of mRNA and Proteins with Subcellular Resolution in Breast Cancer Tissue Samples by Mass Cytometry. Cell Syst. 6, 25–36.e5. 10.1016/j.cels.2017.12.001 [PubMed: 29289569]

Shields J, Kimbler DE, Radwan W, Yanasak N, Sukumari-Ramesh S, Dhandapani KM, 2011. Therapeutic Targeting of Astrocytes After Traumatic Brain Injury. Transl. Stroke Res2, 633–642. 10.1007/s12975-011-0129-6 [PubMed: 24323684]

Stary C, Xu L, Sun X, Ouyang Y-B, White R, Leong J, Li J, Xiong X, Giffard R, 2015. MicroRNA-200c Contributes to Injury From Transient Focal Cerebral Ischemia by Targeting Reelin. Stroke46, 551–556. 10.1161/STROKEAHA.114.007041 [PubMed: 25604249]

Stary CM, Giffard RG, 2015. Advances in Astrocyte-targeted Approaches for Stroke Therapy: An Emerging Role for Mitochondria and microRNAS. Neurochem. Res40, 301–307. 10.1007/s11064-014-1373-4 [PubMed: 24993363]

Stary CM, Sun X, Ouyang Y, Li L, Giffard RG, 2016. miR-29a differentially regulates cell survival in astrocytes from cornu ammonis 1 and dentate gyrus by targeting VDAC1. Mitochondrion30, 248–254. 10.1016/j.mito.2016.08.013 [PubMed: 27553862]

Takahiro Takano, Oberheim NancyAnn Cotrina Maria Luisa, Maiken Nedergaard, 2009. Astrocytes and Ischemic Injury. Stroke40, S8–S12. 10.1161/STROKEAHA.108.533166 [PubMed: 19064795]

Tang M, Liu P, Li X, Wang J, Zhu X, He F, 2017. Protective action of B1R antagonist against cerebral ischemia-reperfusion injury through suppressing miR-200c expression of Microglia derived microvesicles. Neurol. Res39, 612–620. 10.1080/01616412.2016.1275096 [PubMed: 28398146]

Türeyen K, Vemuganti R, Sailor KA, Dempsey RJ, 2004. Infarct volume quantification in mouse focal cerebral ischemia: a comparison of triphenyltetrazolium chloride and cresyl violet staining techniques. J. Neurosci. Methods139, 203–207. 10.1016/j.jneumeth.2004.04.029 [PubMed: 15488233]

Ünal-Çevik I, Kılınç M, Gürsoy-Özdemir Y, Gurer G, Dalkara T, 2004. Loss of NeuN immunoreactivity after cerebral ischemia does not indicate neuronal cell loss: a cautionary note. Brain Res. 1015, 169–174. 10.1016/j.brainres.2004.04.032 [PubMed: 15223381]

Weller ML, Stone IM, Goss A, Rau T, Rova C, Poulsen DJ, 2008. Selective overexpression of excitatory amino acid transporter 2 (EAAT2) in astrocytes enhances neuroprotection from moderate but not severe hypoxia–ischemia. Neuroscience155, 1204–1211. 10.1016/j.neuroscience.2008.05.059 [PubMed: 18620031]

Xiong B, Li A, Lou Y, Chen S, Long B, Peng J, Yang Z, Xu T, Yang X, Li X, Jiang T, Luo Q, Gong H, 2017. Precise Cerebral Vascular Atlas in Stereotaxic Coordinates of Whole Mouse Brain. Front. Neuroanat11. 10.3389/fnana.2017.00128

Xu L, Emery JF, Ouyang Y-B, Voloboueva LA, Giffard RG, 2010. Astrocyte targeted overexpression of Hsp72 or SOD2 reduces neuronal vulnerability to forebrain ischemia. Glia58, 1042–1049. 10.1002/glia.20985 [PubMed: 20235222]

Xu L-J, Ouyang Y-B, Xiong X, Stary CM, Giffard RG, 2015. Post-stroke treatment with miR-181 antagomir reduces injury and improves long-term behavioral recovery in mice after focal cerebral ischemia. Exp. Neurol264, 1–7. 10.1016/j.expneurol.2014.11.007 [PubMed: 25433215]

Yu DS, Lv G, Mei XF, Cao Y, Wang YF, Wang YS, Bi YL, 2015. MiR-200c regulates ROS-induced apoptosis in murine BV-2 cells by targeting FAP-1. Spinal Cord53, 182–189. 10.1038/sc.2014.185 [PubMed: 25448187]

Yuan C, Xu M, Rong R, Mei Y, Cai W, Li L, Xue Y, Zhu B, Sun K, Han L, 2017. miR-200c regulates endothelin-1 induced PASMCs abnormal proliferation and apoptosis. IUBMB Life69, 877–886. 10.1002/iub.1686 [PubMed: 29044995]

Zhang X, Wu F, Jiao Y, Tang T, Yang L, Lu C, Zhang Yanhong, Zhang Yuan, Bai Y, Chao J, Teng G, Yao H, 2017. An Increase of Sigma-1 Receptor in the Penumbra Neuron after Acute Ischemic Stroke. J. Stroke Cerebrovasc. Dis26, 1981–1987. 10.1016/j.jstrokecerebrovasdis.2017.06.013 [PubMed: 28687423]

Zille M, Farr TD, Przesdzing I, Müller J, Sommer C, Dirnagl U, Wunder A, 2012. Visualizing Cell Death in Experimental Focal Cerebral Ischemia: Promises, Problems, and Perspectives. J. Cereb. Blood Flow Metab32, 213–231. 10.1038/jcbfm.2011.150 [PubMed: 22086195]

Highlights:

- Pimonidazole fluorescence multi-complexed with microRNA *in situ* hybridization and protein immunofluorescence represents a novel approach to visualize ischemic regions in the brain.
- Peri-ischemic regions with higher miR-200c areas correlate with areas of neurons susceptible to delayed cell death.
- Targeted inhibition of miR-200c in astrocytes represents a promising precision medicine therapeutic for salvaging penumbra after stroke.

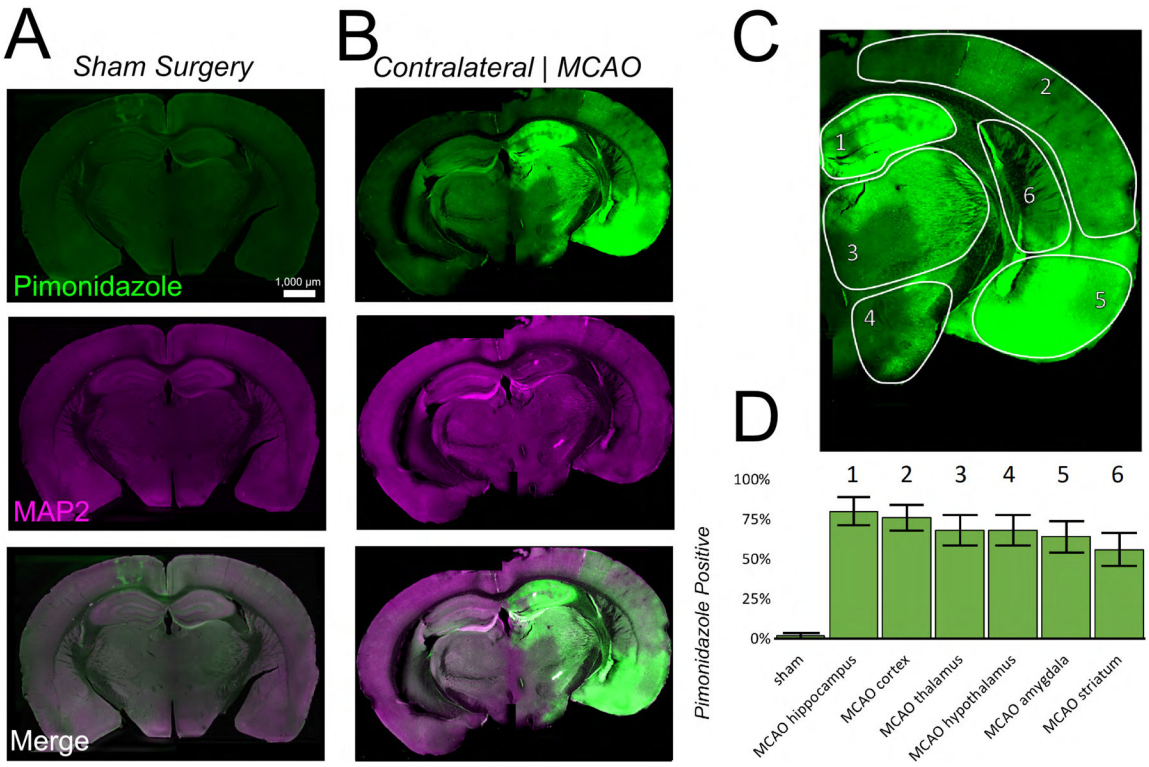

Figure 1. Co-localization of regional ischemia with MAP2 expression after experimental stroke.

A) Representative image of a sham brain with the hypoxia indicator pimonidazole (green) and the neuronal marker micro-tubule associated protein 2 (MAP2, violet). **B)** A representative image of pimonidazole and MAP2 fluorescence 30 min after 1 hr of middle cerebral artery occlusion (MCAO). **C)** The anatomic regions typically visualized by hypoxyprobe at 30 minutes and 2 hrs. 1=cortex, 2=hippocampus, 3=thalamus, 4=hypothalamus, 5=amygdala, 6=striatum. **D)** Semi-quantitative assessment of regional pimonidazole fluorescence after MCAO.

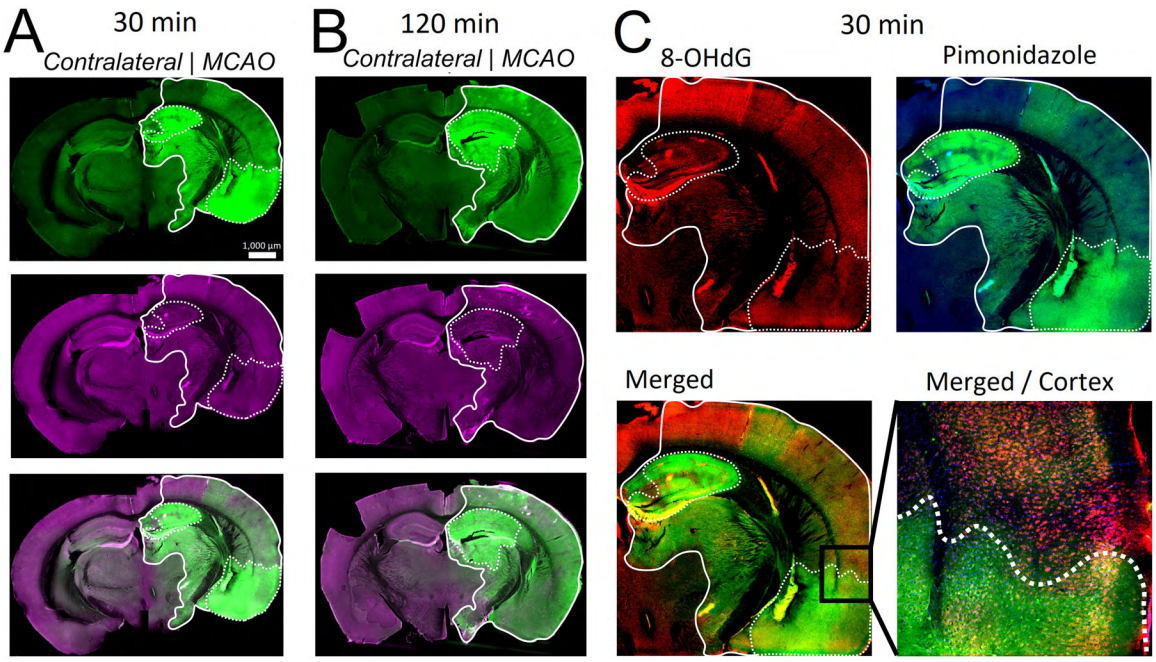

Figure 2. Time course of regional ischemia with pimonidazole and MAP2 expression after experimental stroke.

A representative image of pimonidazole (green) and MAP2 (violet) fluorescence **A)** 30 min and **B)** 2 hrs after 1 hr of middle cerebral artery occlusion (MCAO). Solid lines indicate ischemic regions, and dashed lines delineate severe core forming ischemic regions. **C)** Representative image for ischemic regions (pimonidazole, green – DAPI, blue) with varying severity corresponding to areas of 8-OHdG (red) at 30 minutes after MCAO.

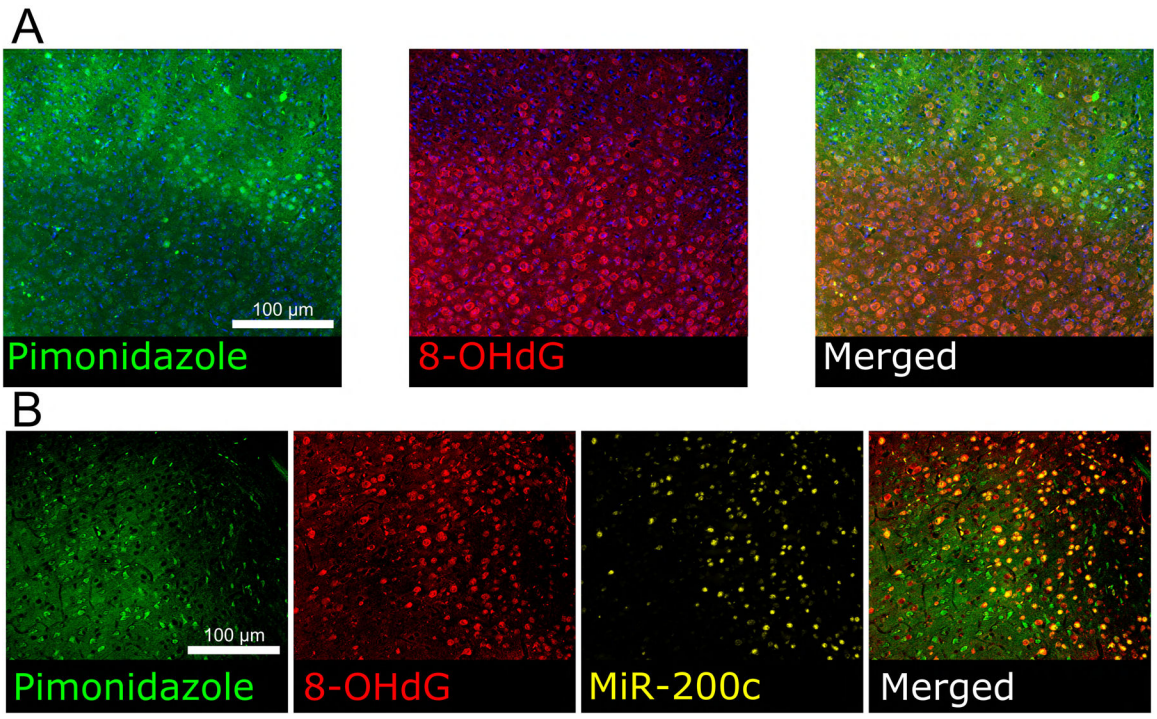

Figure 3. A) Co-localizing oxidative stress and miR-200c expression in core and penumbra after experimental stroke.

Regions where pimonidazole fluorescence (green) was high in intensity representing the ischemic core corresponded to areas of low 8-OHdG fluorescence (red) 2 hrs after MCAO. **B)** Correspondingly, areas of low pimonidazole fluorescence (penumbra) overlapped with high 8-OHdG and greater miR-200c (yellow) expression.

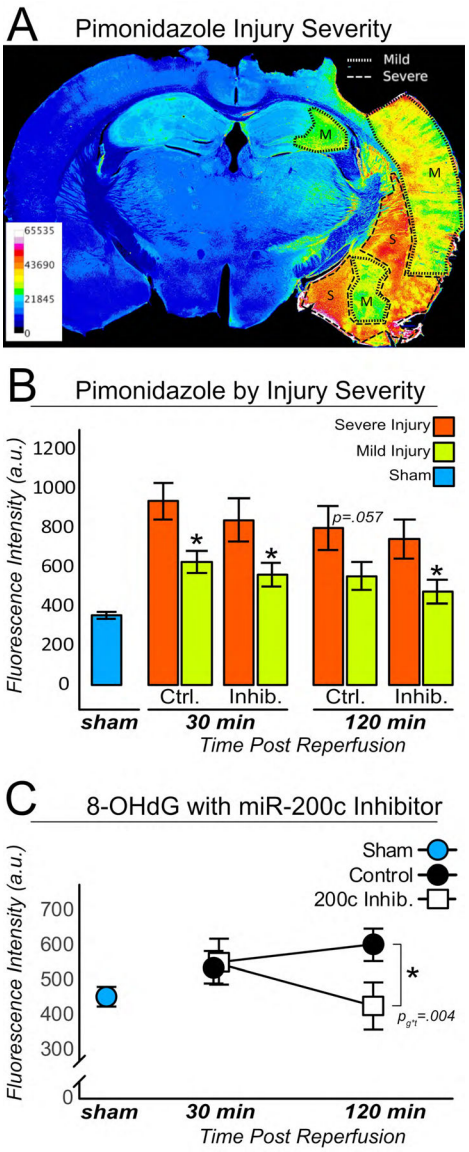

Figure 4. Semi-quantitative assessment of injury severity with pimonidazole fluorescence.

A) Visual heat map of ‘severe’ or ‘mild’ injury in a brain 2 hrs after MCAO by assessment of signal intensity. Uninjured hemispheres did not demonstrate significant variation in signal intensity. **B)** Bar chart depicting mean pimonidazole fluorescence intensity of ‘severe’ and ‘mild’ regions of mismatch-control (Ctrl) and miR-200c antagomir (Inhib) -treated brains at 30 mins and 2 hrs post-reperfusion. **C)** Line graph of 8-OHdG fluorescence in areas of ‘mild’ injury regions determined by multivariate analysis. There was no difference in 8-OHdG fluorescence intensity between the groups after 30 minutes of ischemia [control 532 (486–579), miR-200c antagomir treated 548 (522–574)]. After 120 mins of ischemia the control group had higher 8-OHdG intensity compared to miR-200c treated group, 597 (530–574), and 422 (374–469), respectively (n=4, *p < 0.05; **p < 0.01; ***p < 0.001).

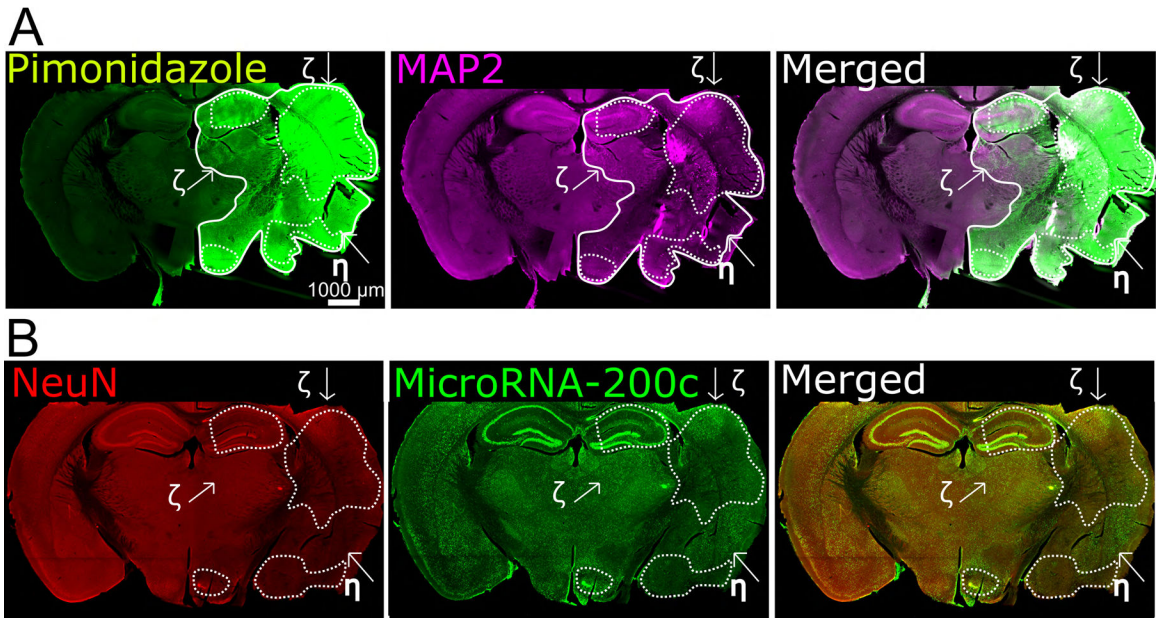

Figure 5. Co-localization of regional expression of pimonidazole fluorescence MAP2, NeuN and miR-200c after MCAO.

A) Pimonidazole fluorescence (green) and MAP2 (violet) in brain 2 hrs after MCAO.

B) Loss of NeuN (red) fluorescence and decreased miR-200c expression co-localize at cortical regions (Ischemic core). ζ = Ischemic areas with no loss of MAP2 or NeuN, and clear miR-200c expression. η = clear ischemic region with loss of NeuN and MAP2, but observable miR-200c expression. ζ and η represent penumbral areas.

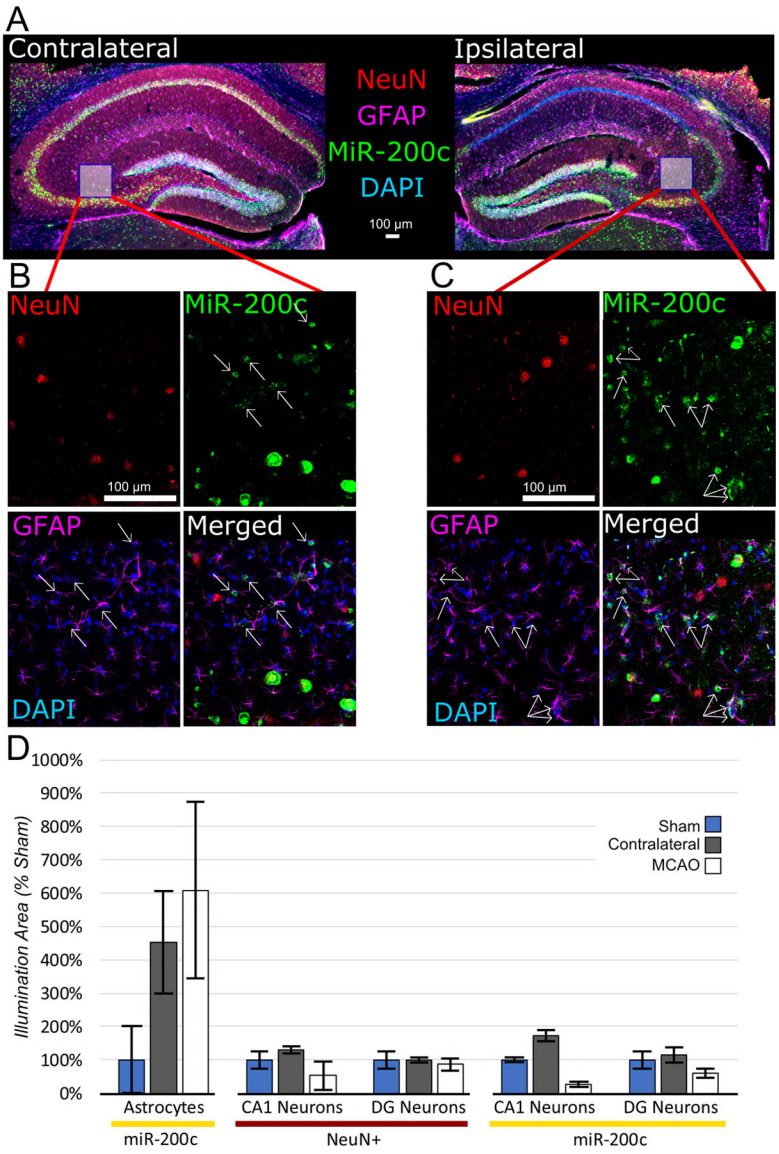

Figure 6. Regional cell-type specific hippocampal expression of miR-200c after MCAO.

A) Contralateral (left) and ipsilateral (right) hippocampi 2 hrs post-MCAO. Ipsilateral hippocampus demonstrates selective loss of NeuN expression. **B)** In contralateral hippocampus the greatest levels of miR-200c expression were evident in NeuN+ cells, whereas GFAP+ astrocytes (indicated by arrows) expressed relatively decreased miR-200c. **C)** In contrast, GFAP+ astrocytes in the ipsilateral side displayed more robust expression of miR-200c (arrows) relative to contralateral astrocytes, while NeuN+ miR-200c expression appeared to relatively decrease in parallel with NeuN immunogenicity. **D)** Semi-quantitative analysis of miR-200c expression in GFAP+ cells and NeuN+ cells. Relative to sham animals miR-200c in astrocytes trended (p=0.052) towards increased expression in ipsilateral hippocampus, contrasting with miR-200c expression in neurons (n=4).